Antitumoral Potential of the Histone Demethylase Inhibitor GSK-J4 in Retinoblastoma

Yanyan Zhang,[1–3] Weiqi Wu,[1–3] Caixia Xu,[1,2] Hongwei Yang,[1,2] and Guofu Huang[1,3,4]

[1]Department of Ophthalmology, The Third Affiliated Hospital of Nanchang University, Nanchang, Jiangxi, PR China
[2]Medical Department of Graduate School, Nanchang University, Nanchang, Jiangxi, PR China
[3]Jiangxi Provincial Key Laboratory of Tumor Metastasis and Precision Therapy, Center Laboratory, The Third Affiliated Hospital of Nanchang University, Nanchang, Jiangxi, PR China
[4]Zhongshan Ophthalmic Center, Sun Yat-Sen University, Guangzhou, Guangdong, PR China

Correspondence: Guofu Huang, Zhongshan Ophthalmic Center, Sun Yat-Sen University, Xianlie South Road 54, Guangzhou, Guangdong 510060, PR China; hgf2222@sina.com.

Received: December 31, 2022
Accepted: January 31, 2024
Published: February 23, 2024

Citation: Zhang Y, Wu W, Xu C, Yang H, Huang G. Antitumoral potential of the histone demethylase inhibitor GSK-J4 in retinoblastoma. *Invest Ophthalmol Vis Sci.* 2024;65(2):34. https://doi.org/10.1167/iovs.65.2.34

Purpose. The purpose of this study was to investigate the antitumor effects of GSK-J4 on retinoblastoma, as well as its related biological functions and molecular mechanisms.

Methods. The antitumor effect of GSK-J4 on retinoblastoma was evaluated by in vitro and in vivo assays. CCK-8, EdU incorporation, and soft agar colony formation assays were performed to examine the effect of GSK-J4 on cell proliferation. Flow cytometry was used to evaluate the effect of GSK-J4 on the cell cycle and apoptosis. RNA-seq and Western blotting were conducted to explore the molecular mechanisms of GSK-J4. An orthotopic xenograft model was established to determine the effect of GSK-J4 on tumor growth.

Results. GSK-J4 significantly inhibited retinoblastoma cell proliferation both in vitro and in vivo, arrested the cell cycle at G2/M phase, and induced apoptosis. Mechanistically, GSK-J4 may suppress retinoblastoma cell growth by regulating the PI3K/AKT/NF-κB signaling pathway.

Conclusions. The antitumor effects of GSK-J4 were noticeable in retinoblastoma and were at least partially mediated by PI3K/AKT/NF-κB pathway suppression. Our study provides a novel strategy for the treatment of retinoblastoma.

Keywords: GSK-J4, retinoblastoma, cell cycle, apoptosis, NF-κB

Retinoblastoma, typically caused by the biallelic mutation of the retinoblastoma gene (RB1), is considered the most prevalent intraocular tumor in childhood worldwide, occurring in approximately 1 out of every 16,000 to 18,000 live births.[1–3] In recent decades, retinoblastoma management has drastically improved, and its goals have evolved from saving life to preserving the globe and currently optimizing vision. Consequently, the survival rates of patients with retinoblastoma have improved in recent years.[4,5] However, children with high-risk clinical features still exhibit poor responses to treatment. This treatment inefficacy can lead to an increase in tumor growth, resulting in impaired vision, globe damage, and even death if metastasis occurs.[6–8] Currently, chemotherapy is the standard retinoblastoma treatment for children with high-risk clinical features, but cases of chemotherapy-induced toxicity have been recently reported.[9–11] Therefore, there is an urgent need to explore novel strategies for the treatment of retinoblastoma.

Histone modification plays a crucial role in the occurrence and progression of cancer, especially histone lysine methylation, which is one of the most characterized histone modifications.[12,13] Tri-methylation of the 27th lysine residue on histone H3 (H3K27me3), one such histone modification, is closely linked to developmentally driven gene silencing and cancer initiation and progression.[14] H3K27me3 demethylation and trimethylation are primarily catalyzed by the 2 members of the KDM6 family of lysine demethylases (UTX, also known as KDM6A, and JMJD3, also known as KDM6B), and the polycomb complex 2 (PRC2) of lysine methyltransferases.[15–17] Notably, the methylation regulation of H3K27me3 (both demethylation and trimethylation) is involved in cellular transformation and cancer cell plasticity,[14,18] and several reports have indicated that PRC2, KDM6A, and KDM6B participate in tumor growth.[19–21] Thus, strategies targeting the regulation of H3K27me3 are especially important for cancer treatment. The utilization of PRC2 inhibitors has been extensively investigated in various cancer models, and several of these inhibitors are currently under clinical evaluation.[22–25] In contrast, research on KDM6 inhibitors has only recently been conducted in some cancers, such as prostate tumors, neuroblastoma, head and neck cancer, and colorectal cancer,[26–29] and most of these inhibitors have shown promising prospects for cancer treatment. However, the effect of KDM6 inhibition on retinoblastoma is still unclear, and the biological functions and molecular mechanisms of KDM6 inhibitors in retinoblastoma remain to be elucidated.

GSK-J4, a selective small-molecule KDM6A/B inhibitor, inhibited H3K27me3 demethylation, and suppressed the abnormal growth of multiple cancers both in vitro and in vivo, including acute myeloid leukemia, glioma, and breast

cancer.[30–36] Nevertheless, it has not yet entered clinical trials, and further expansion of preclinical data is needed. In this study, the therapeutic potential of GSK-J4 in retinoblastoma was explored. We evaluated the effect of GSK-J4 on the biological functions of retinoblastoma cells in vitro and the tumorigenicity of Y79 cells in vivo. Furthermore, the potential molecular mechanisms participating in this process were also explored.

Materials and Methods

Cell Lines and Chemical Reagents

The retinoblastoma cell lines (Y79 and WERI-Rb1) were purchased from the Institute of Biochemistry and Cell Biology (Shanghai, China) and maintained in RPMI 1640 medium (Solarbio, Beijing, China) containing 10% fetal bovine serum (FBS; Gibco, Grand Island, NY, USA) and 1% penicillin/streptomycin (P/S) in an incubator at 37°C with 5% CO_2. GSK-J4 purchased from MedChemExpress of China was dissolved in dimethyl sulfoxide (DMSO; Solarbio, Beijing, China), and 10 mM was used as the initial concentration. Y79 cells were tested with 0.2, 0.4, 0.6, and 0.8 µM GSK-J4, and 0.0001% DMSO (equal amount of DMSO at the highest concentration) was used as a control. WERI-Rb1 cells were tested with 0.6, 1.2, 1.8, and 2.4 µM GSK-J4, and 0.0003% DMSO (equal amount of DMSO at the highest concentration) was used as a control.

Cell Counting Kit-8 Assay

Cell viability was indirectly assessed by CCK-8 assay. Approximately 8000 cells were plated into each well of 96-well plates, and 10 µL CCK-8 reagent (Yeasen, Shanghai, China) was then added after the cells were treated with the drug for 24, 48, or 72 hours. After incubation for 2 hours in the dark, the optical density (OD) value was measured at a wavelength of 450 nm.

5-Ethynyl-2′-Deoxyuridine Cell Proliferation Assay

EdU incorporation was carried out using a Click-iT EdU Alexa Fluor 488 Flow Cytometry Assay Kit (KeyGEN BioTECH, Nanjing, China) according to the manufacturer's instructions. Briefly, the cells were treated with the drug for 72 hours and then incubated with 5 µM EdU for 1 hour. Samples were then fixed and permeabilized with 4% paraformaldehyde and 0.5% Triton X-100, respectively. Next, 1 mL of reaction cocktail was added to each sample and incubated at room temperature for 30 minutes in the dark. Finally, analysis by flow cytometry was performed using the 488 nm excitation green emission filter, and the data were analyzed using FlowJo (version 10; BD FACSCalibur; Becton, Dickinson and Company, Franklin Lakes, NJ, USA).

Soft Agar Colony Formation Assay

This assay was performed using low melting agarose (Biofroxx, Einhausen, Germany) in 6-well plates. Prior to the experiment, 1.2% agarose and 0.7% agarose were kept at 40°C to maintain their liquid state after high-temperature and high-pressure sterilization. For the lower layer, 1 mL of liquid 1.2% agarose was mixed with 1 mL of complete cell culture medium and added to the bottom of a well, and then waiting for 30 minutes at room temperature for the gel to solidify. After the lower layer solidified, the middle layer was prepared. Approximately 2000 cells were added to 1 mL of prewarmed complete cell culture medium and gently mixed to obtain a single-cell suspension. Next, 1 mL of complete cell culture medium (containing cells) and 1 mL of liquid 0.7% agarose were mixed and poured rapidly into a well of the plate. The plate was then left at room temperature for approximately 30 minutes to allow the gel to solidify, forming the middle layer containing cells. After the middle layer solidified, 2 mL of complete culture medium was added, and the medium was changed every 5 days. The cells were incubated at 37°C with 5% CO_2. Two weeks later, the formed colonies were stained with 0.01% crystal violet. Photographs were taken for colony counting.

Cell Cycle and Apoptosis Assays

Cell cycle and apoptosis assays were conducted using a flow cytometry-based approach. For the cell cycle assay, the cells were fixed in 70% ethanol at 4°C for 1 hour after washing with PBS and then suspended in 300 µL PBS containing 3 µL propidium iodide (PI; Sigma–Aldrich, St. Louis, MO, USA) and 3 µL RNase (TIANGEN BIOTECH, Beijing, China). The cells were incubated at room temperature for 20 minutes before flow cytometry analysis, and the results were analyzed using FlowJo software (version 10; BD FACSCalibur; Becton, Dickinson and Company, Franklin Lakes, NJ, USA). For the apoptosis assay, an Annexin V-FITC/PI apoptosis detection kit (KeyGEN BioTECH, Nanjing, China) was used according to the manufacturer's instructions. Briefly, the cells were suspended in binding buffer (300 µL) supplemented with Annexin V-FITC (3 µL) and PI (3 µL) after washing with PBS and then incubated in the dark at room temperature for 10 minutes. Finally, the cells were detected by flow cytometry, and the data were analyzed using FlowJo software (version 10; BD FACSCalibur; Becton, Dickinson and Company, Franklin Lakes, NJ, USA).

Protein Extraction and Western Blotting

The cells were lysed with RIPA buffer containing 1% protease inhibitor (Sigma–Aldrich, St. Louis, MO, USA) on ice for 20 minutes, and the total protein in the lysate was separated by approximately 8% to 12% SDS–polyacrylamide gel electrophoresis (PAGE) and subsequently transferred to polyvinylidene fluoride (PVDF) membranes (Millipore, Billerica, MA, USA). Next, the membranes were blocked with 5% skim milk at room temperature for 2 hours, followed by incubation with primary antibodies at 4°C overnight. The membranes were then incubated with 3% skim milk containing secondary antibodies at room temperature for 1 hour. Finally, the proteins were visualized using an ECL system (KeyGEN, Nanjing, China), and the protein density was analyzed using ImageJ (National Institutes of Health, Bethesda, MD, USA). The primary antibodies used were as follows: Cyclin B1 (Cell Signaling Technology, Danvers, MA, USA), phospho-cdc2 (Cell Signaling Technology, Danvers, MA, USA), cleaved PARP (Cell Signaling Technology, Danvers, MA, USA), cleaved caspase-9 (Cell Signaling Technology, Danvers, MA, USA), PI3K (Cell Signaling Technology, Danvers, MA, USA), phospho-PI3K (Cell Signaling Technology, Danvers, MA, USA), AKT (Abcam, Cambridge, UK), phospho-AKT (Abcam, Cambridge, UK), NF-κB (Servicebio, Wuhan, Hubei), phospho-NF-κB (Servicebio, Wuhan, Hubei), and actin (Proteintech, Beijing, China).

Investigative Ophthalmology & Visual Science

Table. Primers for qPCR

Gene	Forward Primer (5′ → 3′)	Reverse Primer (5′ → 3′)
NSG1	AGTTGGGGAACAATTTCGCAG	GTCTTAGTTTTCACGACCACCTT
TRIB3	AAGCGGTTGGAGTTGGATGAC	CACGATCTGGAGCAGTAGGTG
HMGB3	CCAAAGGGCAAGATGTCCG	TTGACAGGGACCTCTGGGTTT
SRGN	AGGTTATCCTACGCGGAGAG	GTCTTTGGAAAAAGGTCAGTCCT
NFKBIA	CTCCGAGACTTTCGAGGAAATAC	GCCATTGTAGTTGGTAGCCTTCA
PGK1	TGGACGTTAAAGGGAAGCGG	GCTCATAAGGACTACCGACTTGG
GAPDH	GGAGCGAGATCCCTCCAAAAT	GGCTGTTGTCATACTTCTCATGG

RNA Sequencing Analysis

Y79 cells treated with DMSO or 0.8 µM GSK-J4 for 48 hours were lysed using TRIzol reagent (TIANGEN BIOTECH, Beijing, China) and then transported to the Beijing Genomics Institute (BGI) on dry ice for construction of a sequencing library using the BGISEQ-500 platform. Each sample was prepared in triplicate. The BGI Bioinformatics Service System was used to analyze the significance of differentially expressed genes (DEGs) between DMSO- and GSK-J4-treated cells. Genes with a fold change ≥ 2 and Q values < 0.01 were considered significant DEGs. The DEGs were visualized using heatmaps. Moreover, functional annotation of the DEGs was carried out by Kyoto Encyclopedia of Genes and Genomes (KEGG), Gene Ontology (GO), and Gene Set Enrichment Analysis (GSEA).

Quantitative Real-Time PCR

Total RNA was extracted from the cells using TRIzol reagent and reverse transcribed to cDNA using the PrimeScript RT kit with genomic DNA eraser (Takara, Beijing, China) according to the manufacturer's instructions. Quantitative PCR (qPCR) was performed with SYBR Green reagents (Takara, Beijing, China) on a CFX96 Real-Time System. The human GAPDH gene was used as a control. All reactions were conducted in triplicate. The $2^{-\Delta\Delta Ct}$ method was used to calculate the relative mRNA expression. The primer sequences used for qPCR are described in the Table.

Orthotopic Xenograft Experiment

Orthotopic xenografts of retinoblastoma were established in 4- to 5-week-old BALB/c female nude mice (SiPeiFu Biotechnology, Beijing, China) by modifying the procedure described previously.[37–39] Briefly, 2×10^5 Y79 human retinoblastoma cells in 2 microliters of sterile phosphate buffered saline were injected into the vitreous of the left eye through the sclera using a Hamilton syringe with a 33-gauge cannula, which allowed for a small incision and potentially reduced the risk of infection. Special care was taken to prevent lens damage or posterior retinal punctures. Following the injection, the eyes were treated with antibiotic eye drops. Three days after intravitreal transplantation, a fundus image of each mouse was taken using a Retinal Imaging System (Optoprobe, Pontypridd, UK) to confirm the successful transplantation of the injected Y79 cells. A total of 28 mice were used in this study to establish orthotopic xenograft models of retinoblastoma. Five mice without detectable tumors were excluded. Among the remaining 23 mice, 3 mice were kept for observation without any treatment, whereas the other 20 mice were randomly divided into 2 treatment groups, with each treatment group consisting of 10 mice. Treatment in the GSK-J4 group (25 mg/kg) or DMSO group (equal volume of vehicle) was performed via intraperitoneal injection every day for 10 consecutive days. During this period, the body weights of the mice were measured every other day to monitor drug tolerability. After 10 consecutive days of treatment, tumor-burdened eyes were obtained and analyzed for the average tumor area per eye using hematoxylin and eosin (H&E) staining, following the previously described procedure.[38,39] Briefly, representative sections spanning the whole eye globe were selected for H&E staining per eye by taking every 50th section (4-µm-thick each) from one end of the eyeball to the other end. The image of each section was then used to quantify the tumor area in pixels using ImageJ software (National Institutes of Health, Bethesda, MD, USA). The tumor burden per mouse was calculated by taking the average tumor area per section from the sections representing different levels of the whole eyeball. Additionally, some of the xenograft sections underwent immunohistochemical staining with a Ki-67 antibody (MedChemExpress, Shanghai, China). All animal experiments were performed according to protocols approved by Nanchang University (KY2023035) and adhered to the standards set forth in the ARVO Statement for the Use of Animals in Ophthalmic and Vision Research, including ensuring all efforts to minimize suffering.

Hematoxylin and Eosin and Immunohistochemistry Staining

The whole eye globe, fixed with 4% paraformaldehyde (Servicebio, Wuhan, Hubei) for more than 24 hours, was embedded in paraffin and processed into 4-µm sections. The sections were then stained with H&E. For immunohistochemistry (IHC) staining, the sections were deparaffinized in xylene, rinsed in ethanol, and rehydrated. Next, antigen retrieval and endogenous peroxidase blocking were performed with Tris-EDTA buffer and 3% H_2O_2 solution as described in the manufacturer's protocols. The appropriate primary antibody was added and incubated at 4°C overnight, followed by incubation with the corresponding secondary antibody (ZSGB-BIO, Beijing, China) at 37°C for 30 minutes. Subsequently, the sections were stained with DAB (3,3′-diaminobenzidine) and counterstained with hematoxylin. The sections were then sealed and observed under a microscope.

Statistical Analysis

Statistical analyzes were performed by GraphPad Prism (version 5.0; GraphPad Software, La Jolla, CA, USA) using unpaired Student's *t*-test and 2-way ANOVA. Each experiment was independently repeated at least three times, and

the data are shown as the mean ± standard deviation (SD). Differences were considered significant at $P < 0.05$.

Results

GSK-J4 Effectively Reduces the Proliferation of Retinoblastoma Cells

To evaluate the effect of GSK-J4 on the growth of retinoblastoma cells, a CCK-8 assay was performed after the cells were treated with different concentrations of GSK-J4 for 24 to 72 hours. The results showed that the viability of Y79 and WERI-Rb1 cells was effectively reduced by GSK-J4 in a concentration-dependent manner (Supplementary Figs. S1A, S1B, Figs. 1A, 1B). The IC50 value of GSK-J4 for Y79 cells was 0.68 µM, whereas that for WERI-Rb1 cells was 2.15 µM at 48 hours. Furthermore, GSK-J4 inhibited retinoblastoma cell proliferation in a time-dependent manner (Figs. 1C, 1D). The EdU incorporation assay also confirmed that the proliferation of retinoblastoma cells was suppressed by GSK-J4 (Figs. 1E–1G). Compared with that in the DMSO-treated group, the proportion of EdU-positive cells in the GSK-J4-treated group significantly decreased, indicating that there were fewer newly generated cells. Consistently, the colony formation ability of retinoblastoma cells was strongly reduced after GSK-J4 treatment. The colony numbers of retinoblastoma cells treated with different concentrations of GSK-J4 were apparently reduced compared to those treated with DMSO (Figs. 1H, 1I, Supplementary Fig. S1C). These results indicated that GSK-J4 efficaciously suppressed retinoblastoma cell proliferation.

GSK-J4 Induced G2/M Cycle Arrest in Retinoblastoma Cells

After the inhibition of retinoblastoma cell proliferation by GSK-J4 was determined, we hypothesized that it correlated with the cell cycle. Retinoblastoma cells were treated with DMSO or different concentrations of GSK-J4 for 48 hours and were then subjected to flow cytometry and Western blotting. The results are shown in Figure 2. The percentage of retinoblastoma cells in the G2/M phase grad-

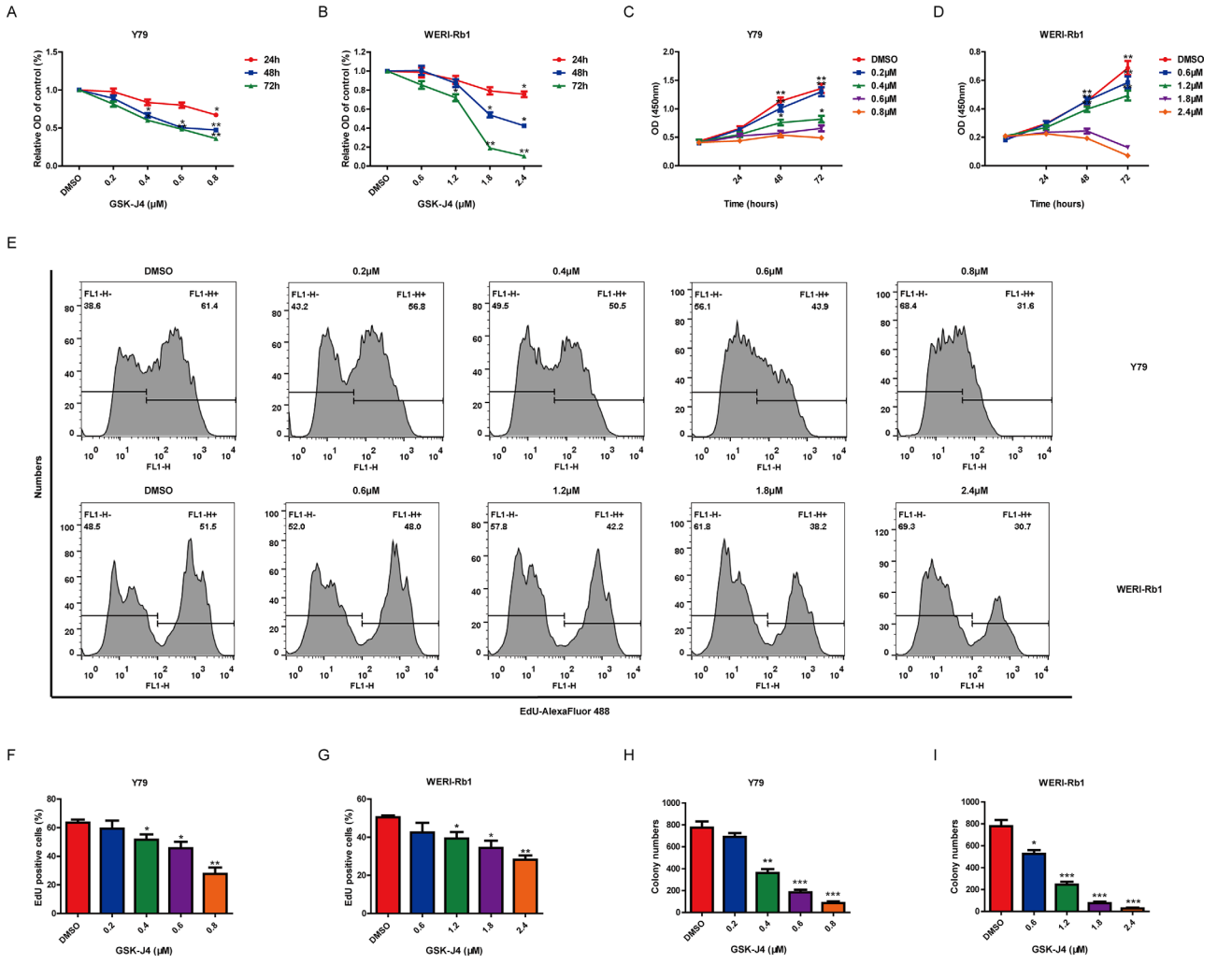

Figure 1. Treatment with GSK-J4 reduced the proliferation of retinoblastoma cells. (**A–D**) Cell viability of Y79 and WERI-Rb1 cells treated with DMSO or GSK-J4 for 24 to 72 hours assessed by the CCK-8 assay. (**E–G**) Flow cytometric analysis of EdU incorporation in Y79 cells and WERI-Rb1 cells treated with DMSO or GSK-J4 for 72 hours. The data were analyzed using FlowJo and GraphPad Prism. (**H**, **I**) Colony numbers from the soft agar colony formation assay on Y79 and WERI-Rb1 cells treated with DMSO or GSK-J4 for 2 weeks (*$P < 0.05$, **$P < 0.01$, ***$P < 0.001$).

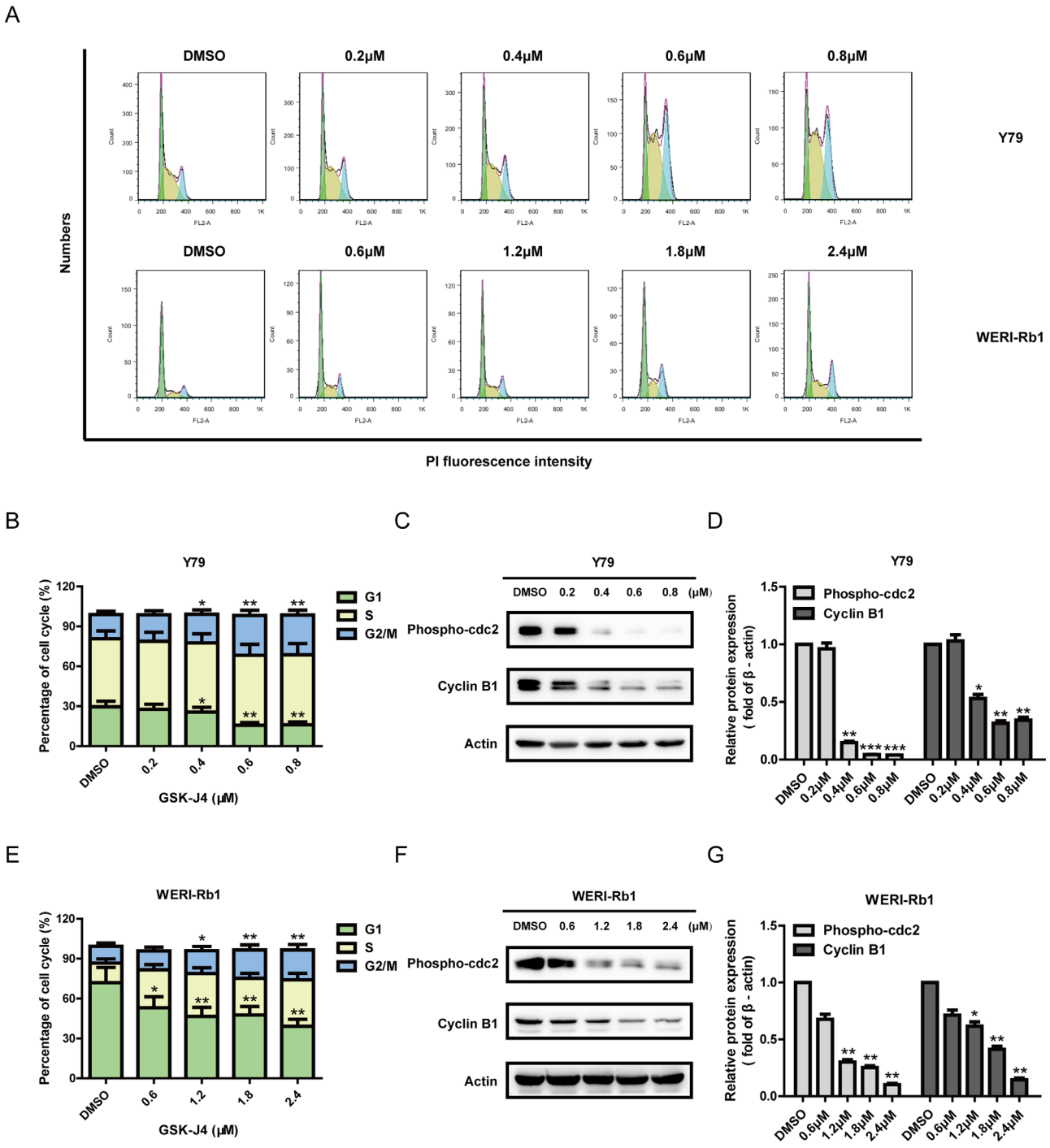

Figure 2. GSK-J4 induced cell cycle arrest at the G2/M phase in retinoblastoma cells. (**A, B, E**) Flow cytometric analysis of the cell cycle in Y79 and WERI-Rb1 cells treated with DMSO or GSK-J4 for 48 hours. The data were analyzed using FlowJo and GraphPad Prism. (**C, D, F, G**) The expression of G2/M checkpoint proteins (phospho-cdc2 and Cyclin B1) examined by Western blotting after DMSO or GSK-J4 treatment for 48 hours in Y79 and WERI-Rb1 cells. The protein densities were analyzed with ImageJ (*$P < 0.05$, **$P < 0.01$, ***$P < 0.001$).

ually increased as the GSK-J4 dose increased, and the percentage of cells in the G1 phase decreased accordingly (see Figs. 2A, 2B, 2E). Thus, GSK-J4 caused cell cycle arrest in the G2/M phase in retinoblastoma cells. Moreover, the expression levels of G2/M checkpoint proteins (phospho-cdc2 and Cyclin B1) were obviously decreased after GSK-J4 treatment (Figs. 2C, 2D, 2F, 2G), further confirming that GSK-J4 arrested the cell cycle at the G2/M phase in retinoblastoma cells. Altogether, the results indicate that GSK-J4 suppressed retinoblastoma cell growth partly through G2/M cycle arrest.

GSK-J4 Promoted the Apoptosis of Retinoblastoma Cells

To further explore the mechanism by which GSK-J4 reduces the viability of retinoblastoma cells, the cell apoptosis was examined by flow cytometry following DMSO or GSK-J4

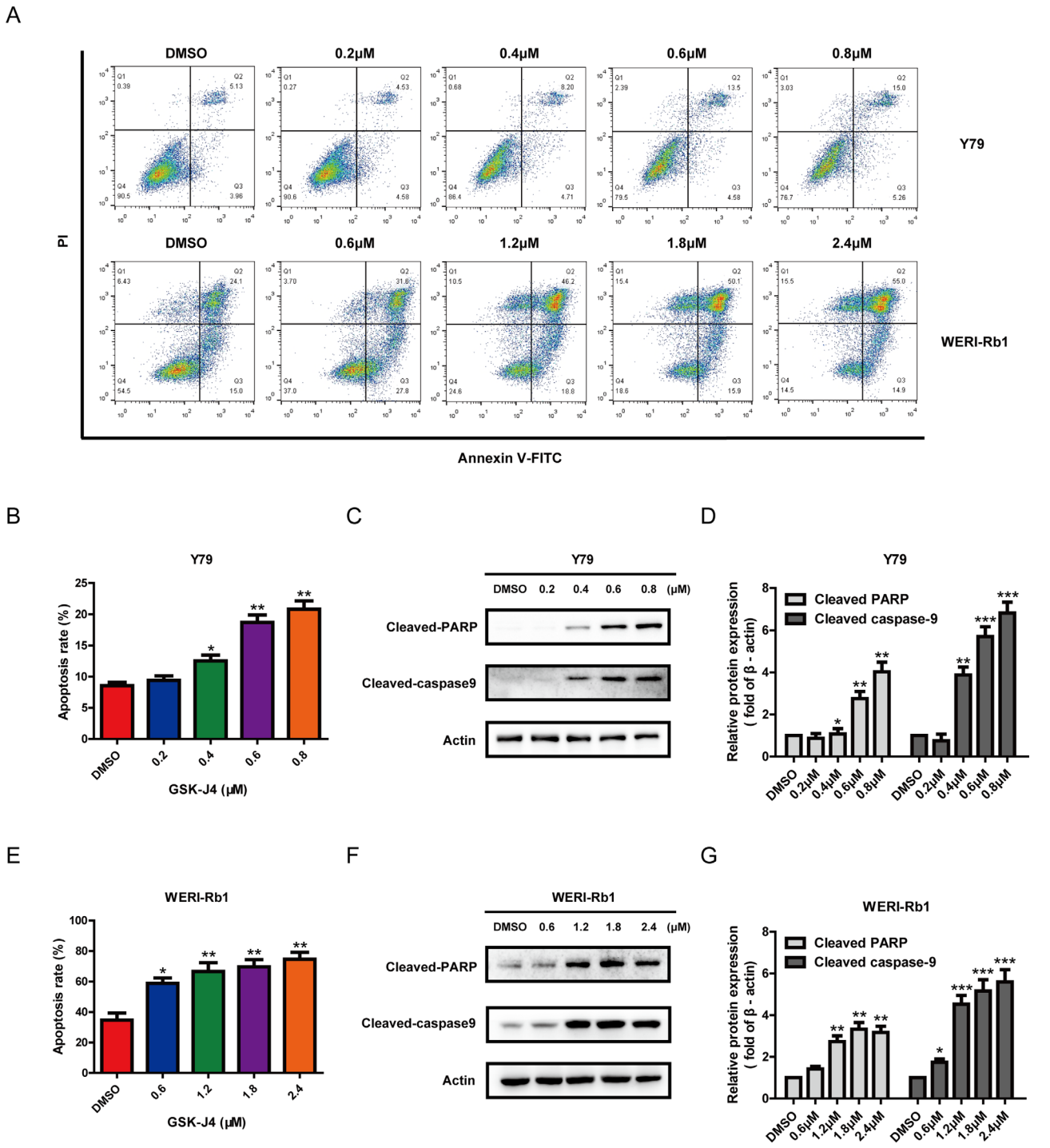

Figure 3. The apoptosis of retinoblastoma cells was promoted by GSK-J4. (**A, B, E**) Flow cytometric analysis of apoptosis in Y79 and WERI-Rb1 cells treated with DMSO or GSK-J4 for 48 hours. The data were analyzed using FlowJo and GraphPad Prism. (**C, D, F, G**) Western blot analysis of apoptosis-related protein (cleaved PARP and cleaved caspase-9) expression in retinoblastoma cells treated with DMSO or GSK-J4 for 48 hours (*$P < 0.05$, **$P < 0.01$, ***$P < 0.001$).

treatment for 48 hours. Compared with DMSO treatment, GSK-J4 treatment significantly increased the proportion of apoptotic cells (Figs. 3A, 3B, 3E). Moreover, apoptosis-related protein expression in retinoblastoma cells treated with DMSO or different concentrations of GSK-J4 for 48 hours was examined by Western blotting. As expected, cleaved PARP and cleaved caspase-9 expression was upregulated (Figs. 3C, 3D, 3F, 3G), indicating that apoptosis was promoted, which was consistent with the flow cytometry results. All of these results suggested that GSK-J4 promoted the apoptosis, thereby inhibiting the proliferation of retinoblastoma cells.

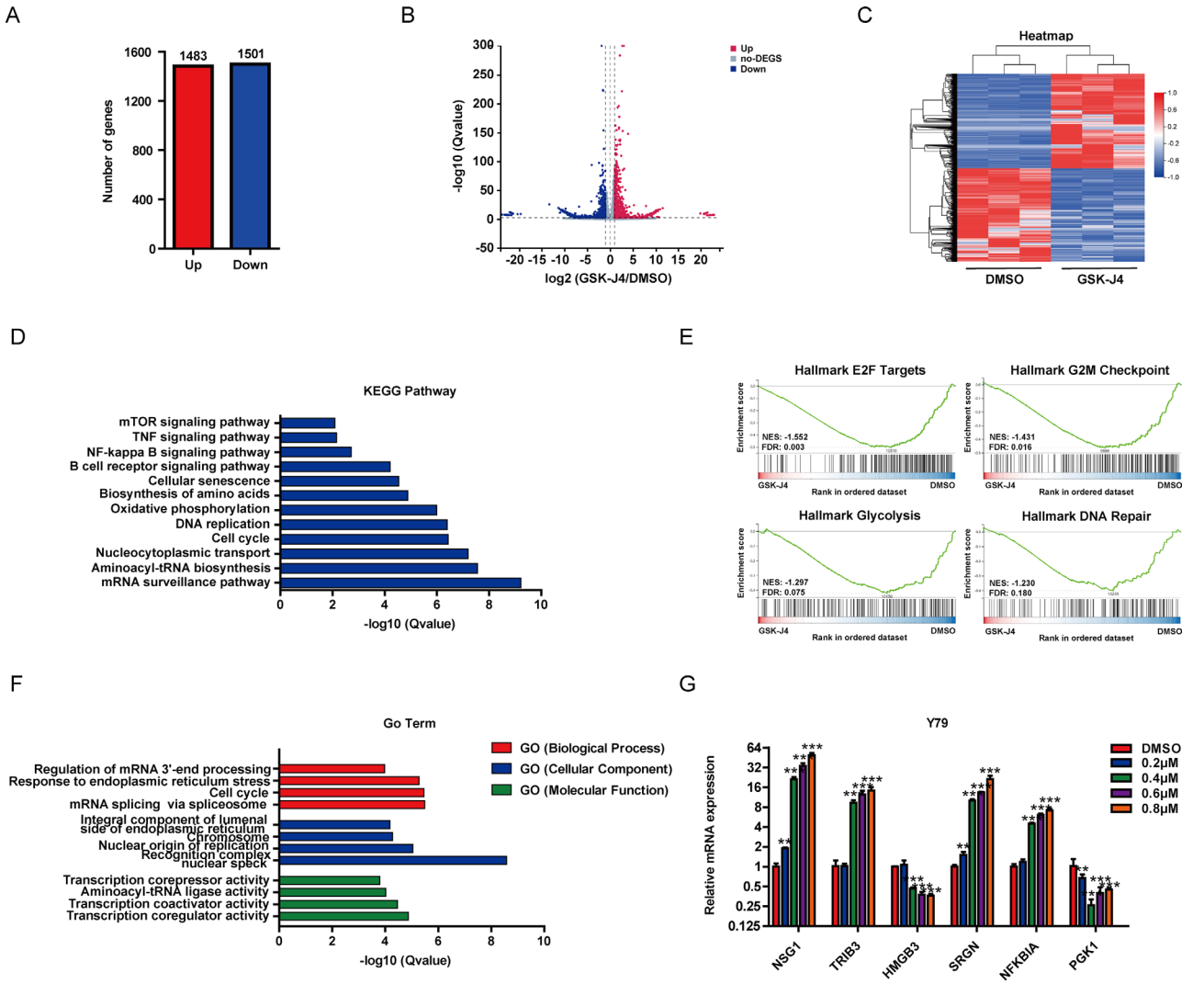

Figure 4. Differentially expressed genes (DEGs) in Y79 cells treated with 0.8 μM GSK-J4 for 48 hours. (**A**) The numbers of upregulated and downregulated genes in GSK-J4-treated Y79 cells compared to DMSO-treated cells. (**B**) A volcano plot showing the DEGs identified from the RNA-seq analysis of Y79 cells treated with DMSO or GSK-J4. (**C**) Heatmap showing the expression levels of the DEGs described in (**A**). (**D, E, F**) Results of KEGG, GSEA (FDR ≤ 0.25 was considered as statistically significant. NES, normalized enrichment score) and GO analysis of the DEGs described in (**A**). (**G**) RT–qPCR analysis of four upregulated genes (NSG1, TRIB3, SRGN, and NFKBIA) and two downregulated genes (HMGB3 and PGK1) (**$P < 0.01$, ***$P < 0.001$).

Gene Expression Changes Induced by GSK-J4

To evaluate the global transcriptional changes associated with GSK-J4 exposure and further explore the molecular mechanism underlying GSK-J4-induced tumor suppression, Y79 cells were treated with 0.8 μM GSK-J4 for 48 hours and then subjected to RNA-seq. Transcriptome analysis results showed that GSK-J4 treatment upregulated 1483 genes and downregulated 1501 genes (Log_2 fold-change ≥ 1 and Q values < 0.01; Figs. 4A–4C). KEGG pathway analysis revealed that the DEGs were mostly enriched in cancer-related pathways, such as the NF-kappa B (NF-κB) signaling pathway, cell growth and death, replication and repair, and energy metabolism (Fig. 4D). This result was further supported by GSEA and GO analysis (Figs. 4E, 4F). RT–qPCR was performed to confirm four upregulated genes (NSG1, TRIB3, SRGN, and NFKBIA) and two downregulated genes (HMGB3 and PGK1), and the results were consistent with the RNA-seq results (Fig. 4G).

GSK-J4 Suppressed the PI3K/AKT/NF-κB Signaling Pathway in Retinoblastoma Cells

Based on the results of RNA-seq analysis, the PI3K/AKT/NF-κB signaling pathway, which plays an important role in the occurrence and development of cancer, was investigated to better understand the mechanism by which GSK-J4 exert an antitumor effect on retinoblastoma cells. A Western blot analysis was performed to evaluate the expression of PI3K/AKT/NF-κB signaling pathway markers after treating retinoblastoma cells with different concentrations of GSK-J4 for 48 hours. As shown in Figures 5A–5C, with increasing GSK-J4 concentration, the protein levels of phospho-PI3K, phospho-AKT, and phospho-NF-κB in retinoblastoma cells were concomitantly decreased, meaning that

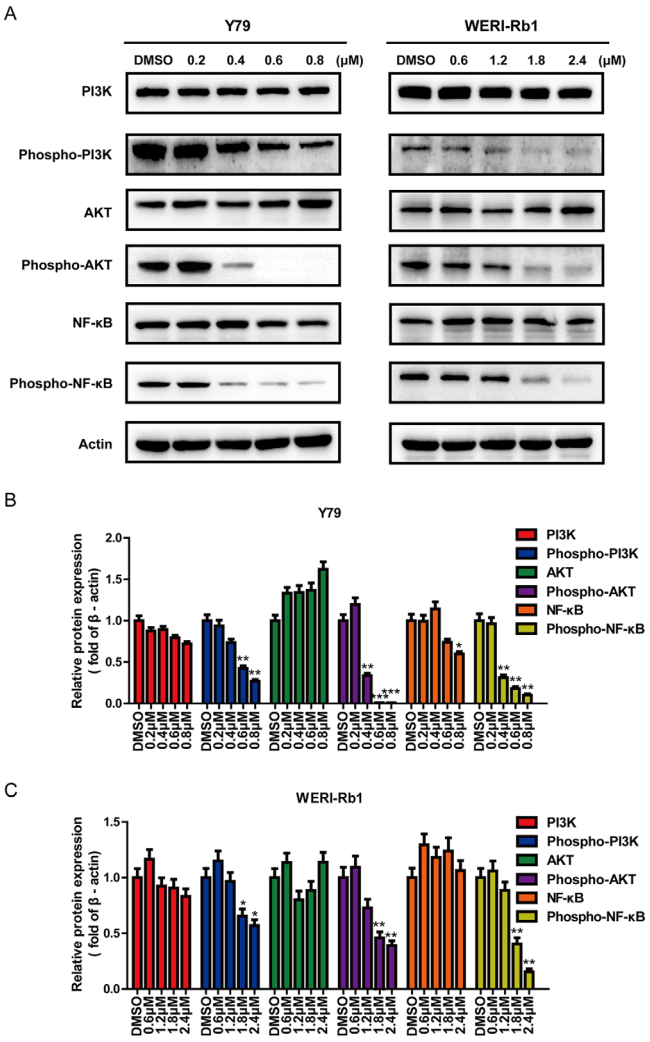

Figure 5. GSK-J4 inhibited the PI3K/AKT/NF-κB signaling pathway in retinoblastoma cells. (**A**) Western blot analysis of PI3K/AKT/NF-κB signaling pathway-related protein expression in Y79 and WERI-Rb1 cells treated with DMSO or GSK-J4 for 48 hours. (**B, C**) Density analysis of proteins in (**A**) ($^{*}P < 0.05$, $^{**}P < 0.01$, $^{***}P < 0.001$).

the PI3K/AKT/NF-κB signaling pathway was suppressed by GSK-J4. Collectively, these results suggested that GSK-J4 might exert its antitumor effects on retinoblastoma cells by regulating the PI3K/AKT/NF-κB signaling pathway.

GSK-J4 Decelerated Tumor Growth in Orthotopic Xenografts of Retinoblastoma

To confirm the effect of GSK-J4 on tumor growth in vivo, an orthotopic xenograft model was established using Y79 cells (Figs. 6A, 6B). Three days after transplantation, tumor establishment in the xenografted mice was examined through retinal imaging (Fig. 6C). Only the mice with detectable tumors were included in the study. The untreated xenografts developed conspicuous tumors over 2 to 3 weeks after transplantation, as shown in Figure 6D. The tumor-burdened eyes after 10 consecutive days of treatment were collected and sliced, followed by H&E staining to analyze the average tumor areas. As shown in Figures 6E and 6F, the average xenograft tumor areas in the GSK-J4 group were significantly smaller than those in the DMSO group, whereas there was no obvious difference in the average body weight of nude mice between the DMSO and GSK-J4 groups during the treatment period (Fig. 6H). Moreover, the expression of Ki-67, which was determined by immunohistochemistry, in the GSK-J4 group was downregulated compared to that in the DMSO group (Fig. 6G). These findings demonstrated that GSK-J4 significantly suppressed retinoblastoma growth in vivo without being particularly toxic to mice at the curative dose.

Discussion

Histone modification plays important and specific roles in cancer development and may provide a new direction for cancer treatment.[40] H3K27me3, the trimethylation of H3 on lysine 27, is one such modification and is controlled by histone methyltransferases (PRC2) and demethylases (KDM6A/B). It has been reported that the dysregulation of H3K27me3 (whether methylated or demethylated) is closely associated with cancer development and progression,[41] thus strategies that keep the H3K27me3 level balance may be a novel strategy for cancer treatment. GSK-J4, a selective inhibitor of KDM6A/B, which are usually aberrantly expressed in cancers, has been found to have significant antitumor efficacy in several cancers.[26,30,42,43] However, the roles of GSK-J4 in retinoblastoma remain unclear. In the present study, we performed CCK-8, EdU incorporation and colony formation assays and found that GSK-J4 obviously inhibited the proliferation of retinoblastoma cells in a concentration- and time-dependent manner. Similarly, tumor growth in the orthotopic xenograft model was also limited after GSK-J4 treatment without affecting the body weight of the animals. This finding supports the potential of GSK-J4 as a novel regimen for the treatment of retinoblastoma.

In our orthotopic xenograft experiment, 2×10^5 numbers of Y79 cells were used for intra-vitreous injection, as referenced in the studies by Mao Y. et al.[38] and Kim J. K. et al.,[39] where our experimental technique conditions and design were similar with theirs. However, we observed that the tumors were formed on the third day after injection, which differed from the results of Kim J. K. et al. and Mao Y. et al. This discrepancy may be attributed to differences in cell culture conditions, the derivation and age of mice, and variations in the injection operation technicians. Therefore, we made an adjustment to the experimental protocol, initiating tumor detection and treatment at the early stage. It allowed to short the entire experimental period, preventing the excessive tumor burden that causes unnecessary suffering and negative impacts on the mice. In addition, due to limitations in experimental technology, we did not have access to accurate monitoring of tumor progression in vivo using techniques such as bioluminescence monitoring with the In Vivo Imaging System (IVIS).[44,45] Consequently, we had to rely on postmortem histopathology to evaluate tumor progression, which may not be the most optimal approach. Specifically, tumor burden per mouse was calculated by taking the average tumor area per section from the H&E staining sections representing different levels of the whole eyeball. However, it is important to note that this method may have certain limitations in terms of accuracy.

As a potential anticancer agent, GSK-J4 has been reported to significantly affect cell growth by influencing the cell cycle.[46] Notably, in different types of cancer (even within

Investigative Ophthalmology & Visual Science

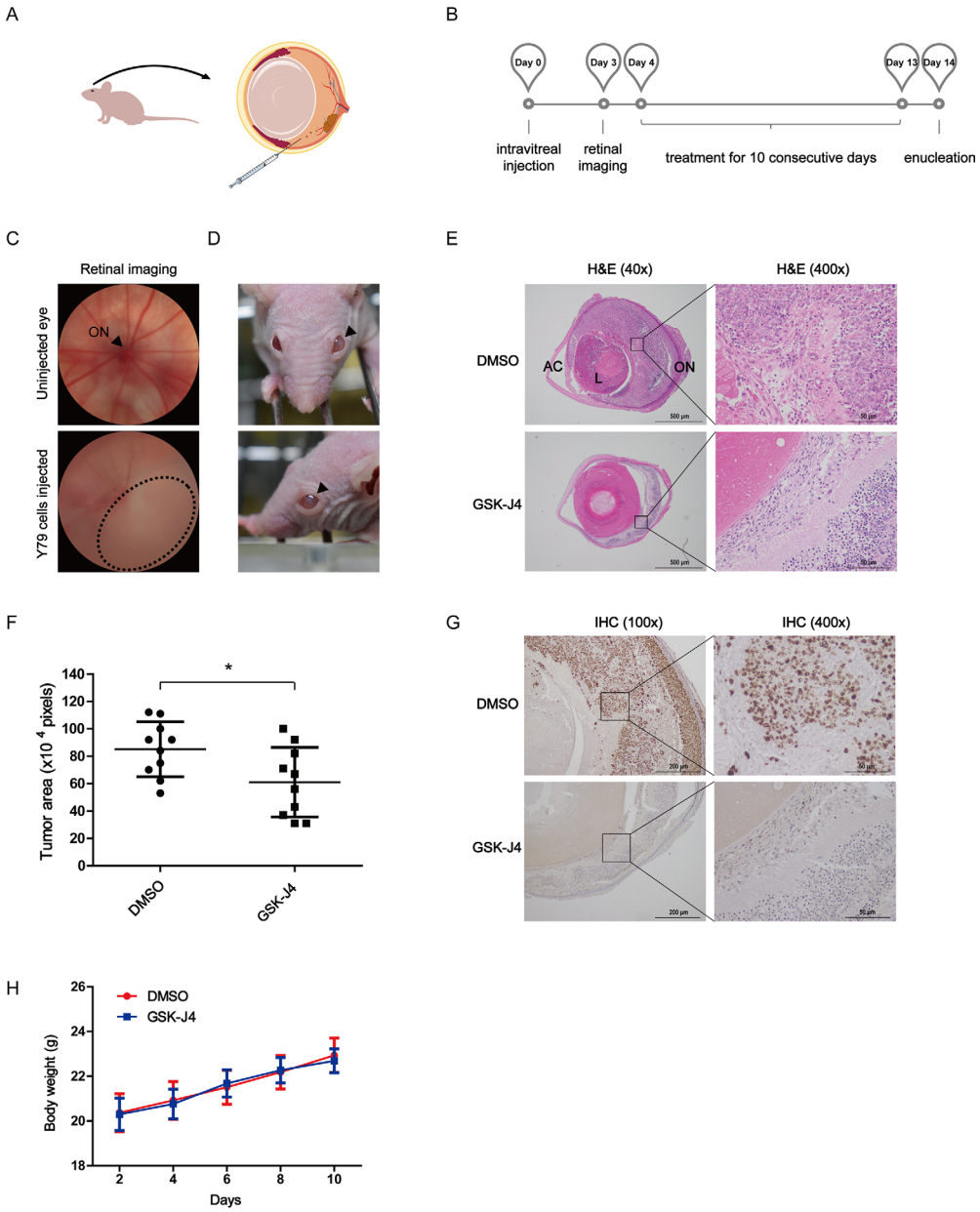

Figure 6. The antitumor efficacy of GSK-J4 in the Y79 orthotopic xenograft model. (**A, B**) Schematic of the orthotopic xenograft study. (**C**) Retinal imaging conducted on day 3 after the transplantation of Y79 cells to examine tumor formation. Xenografted eyes displayed cloud-like tumors, outlined by dotted lines, whereas uninjected eyes showed a clear retinal view. ON, optic nerve. (**D**) Conspicuous tumors in xenografted eyes indicated by an *arrowhead*. (**E**) Hematoxylin and eosin staining of tumor-burdened eyes from the DMSO group and the GSK-J4 group. Scale bars = 500 µm and 50 µm, respectively. AC, anterior chamber; L, lens; ON, optic nerve. (**F**) Plot of tumor areas in the DMSO group and the GSK-J4 group. Data points on the plot represent the average tumor area per mouse. (**G**) Immunohistochemical staining for Ki-67 in xenograft tumor sections from the DMSO group and the GSK-J4 group. Scale bars = 200 µm and 50 µm, respectively. (**H**) Body weight of the mice during treatment (*$P < 0.05$).

different cell lines of the same cancer), the cell cycle phases arrested by GSK-J4 vary. In acute myeloid leukemia, GSK-J4 significantly arrested the cell cycle at the G0/G1 phase in the Kasumi-1 cell line, whereas it arrested the cell cycle at the S phase in the KG-1a cell line.[30,43] In KRAS-mutant anaplastic thyroid cancer, GSK-J4 treatment resulted in the blocking of Cal-62 cells at the G2/M and S phases.[33] In prostate cancer, GSK-J4 arrested both PC3 and C42B cells at the sub-G0-G1 phase.[47] In the present study, the cell cycle of retinoblastoma cells (both Y79 and WERI-Rb1) treated with GSK-J4 was significantly arrested at the G2/M phase, inhibiting cell entry into mitosis, which prevented cell growth. This finding was further supported by the downregulation of Cyclin B1 and the suppression of cdc2 phosphorylation (the critical components of the G2/M checkpoint).[48] Previous research noted that cell cycle arrest always emerges along with cell apoptosis in cancer therapeutic strategies.[49–51] Accordingly, GSK-J4 has been reported to induce cell apoptosis in multiple cancers, partially through the activation of cleaved caspase-3, cleaved caspase-9, and cleaved PARP (the action-

ers of programmed cell death[52,53]).[31,34,36,43,47,54] As expected, retinoblastoma cell apoptosis was triggered by GSK-J4 in a concentration-dependent manner. Moreover, caspase-9 and PARP, the critical participants in the process of apoptosis as previously mentioned,[52,53] were proteolytically activated. These results were consistent with previous findings. Altogether, these data suggested that GSK-J4 reduced the proliferation of retinoblastoma cells via cell cycle arrest and apoptosis promotion.

Several mechanisms of the antiproliferative effects of GSK-J4 have been elucidated in other cancers, including the inhibition of the PKC-a/p-Bcl2 pathway and the suppression of epithelial-mesenchymal transition (EMT) induced by TGF-β.[43,55] In our study, KEGG pathway enrichment analysis and Western blot analysis results revealed that the activation of the NF-κB signaling pathway was inhibited by GSK-J4 in retinoblastoma. Furthermore, PI3K/AKT signaling, a major upstream element of the NF-κB signaling pathway,[56,57] was also suppressed under GSK-J4 treatment. GSK-J4 may exert its antitumor effect on retinoblastoma cells, at least partially, via the PI3K/AKT/NF-κB signaling pathway. It offers new insight into the understanding of the antitumor mechanism of GSK-J4.

Our results, coupled with previous research findings, suggested that GSK-J4 effectively inhibits cancer growth and progression both in vitro and in vivo.[46] In addition, in vivo studies also showed the suitable tolerance of GSK-J4 in mice.[26,29,30] Moreover, some studies have indicated that GSK-J4 could enhance the effectiveness of known anticancer drugs when used in combination.[33,43,58] Although promising, these results are still preliminary, and further investigations involving more extensive research and clinical trials will be considered soon, similar to other strategies targeting the regulation of H3K27me3, such as PRC2 inhibitors, which have been well studied and entered multiple clinical trials.[22–25]

In conclusion, our findings showed that GSK-J4 effectively reduced retinoblastoma cell growth, which was probably mediated by the inhibition of the PI3K/AKT/NF-κB signaling pathway. Moreover, GSK-J4 may serve as a potential chemotherapeutic strategy for the treatment of retinoblastoma in the future.

Acknowledgments

Supported by the National Natural Science Foundation of China (No. 82060501 to H.G.F.), the Natural Science Foundation of Jiangxi Province (No. 20202ACB206005 to H.G.F.).

Disclosure: **Y. Zhang**, None; **W. Wu**, None; **C. Xu**, None; **H. Yang**, None; **G. Huang**, None

References

1. Dimaras H, Corson TW, Cobrinik D, et al. Retinoblastoma. *Nat Rev Dis Primers*. 2015;1:15021.
2. Little MP, Kleinerman RA, Stiller CA, Li G, Kroll ME, Murphy MF. Analysis of retinoblastoma age incidence data using a fully stochastic cancer model. *Int J Cancer*. 2012;130:631–640.
3. Fernandes AG, Pollock BD, Rabito FA. Retinoblastoma in the United States: a 40-year incidence and survival analysis. *J Pediatr Ophthalmol Strabismus*. 2018;55:182–188.
4. Ancona-Lezama D, Dalvin LA, Shields CL. Modern treatment of retinoblastoma: a 2020 review. *Indian J Ophthalmol*. 2020;68:2356–2365.
5. Munier FL, Beck-Popovic M, Chantada GL, et al. Conservative management of retinoblastoma: challenging orthodoxy without compromising the state of metastatic grace. "Alive, with good vision and no comorbidity". *Prog Retin Eye Res*. 2019;73:100764.
6. Kaliki S, Srinivasan V, Gupta A, Mishra DK, Naik MN. Clinical features predictive of high-risk retinoblastoma in 403 Asian Indian patients: a case-control study. *Ophthalmology*. 2015;122:1165–1172.
7. Kaliki S, Mittal P, Mohan S, et al. Bilateral advanced (group D or E) intraocular retinoblastoma: outcomes in 72 Asian Indian patients. *Eye (Lond)*. 2019;33:1297–1304.
8. Kumar A, Moulik NR, Mishra RK, Kumar D. Causes, outcome and prevention of abandonment in retinoblastoma in India. *Pediatr Blood Cancer*. 2013;60:771–775.
9. Chevez-Barrios P, Eagle RC, Jr., Krailo M, et al. Study of unilateral retinoblastoma with and without histopathologic high-risk features and the role of adjuvant chemotherapy: a children's oncology group study. *J Clin Oncol*. 2019;37:2883–2891.
10. Gombos DS, Hungerford J, Abramson DH, et al. Secondary acute myelogenous leukemia in patients with retinoblastoma: is chemotherapy a factor? *Ophthalmology*. 2007;114:1378–1383.
11. Soliman SE, D'Silva CN, Dimaras H, Dzneladze I, Chan H, Gallie BL. Clinical and genetic associations for carboplatin-related ototoxicity in children treated for retinoblastoma: a retrospective noncomparative single-institute experience. *Pediatr Blood Cancer*. 2018;65:e26931.
12. Cao YC, Shan SK, Guo B, et al. Histone lysine methylation modification and its role in vascular calcification. *Front Endocrinol (Lausanne)*. 2022;13:863708.
13. Bannister AJ, Kouzarides T. Regulation of chromatin by histone modifications. *Cell Res*. 2011;21:381–395.
14. Das P, Taube JH. Regulating methylation at H3K27: a trick or treat for cancer cell plasticity. *Cancers (Basel)*. 2020;12:2792.
15. Xia J, Li J, Tian L, Ren X, Liu C, Liang C. Targeting enhancer of Zeste homolog 2 for the treatment of hematological malignancies and solid tumors: candidate structure-activity relationships insights and evolution prospects. *J Med Chem*. 2022;65:7016–7043.
16. Tran N, Broun A, Ge K. Lysine demethylase KDM6A in differentiation, development, and cancer. *Mol Cell Biol*. 2020;40:e00341–e00420.
17. Sanchez A, Houfaf Khoufaf FZ, Idrissou M, et al. The functions of the demethylase JMJD3 in cancer. *Int J Mol Sci*. 2021;22:968.
18. Day CA, Hinchcliffe EH, Robinson JP. H3K27me3 in diffuse midline glioma and epithelial ovarian cancer: opposing epigenetic changes leading to the same poor outcomes. *Cells*. 2022;11:3376.
19. Volkel P, Dupret B, Le Bourhis X, Angrand PO. Diverse involvement of EZH2 in cancer epigenetics. *Am J Transl Res*. 2015;7:175–193.
20. Benyoucef A, Palii CG, Wang C, et al. UTX inhibition as selective epigenetic therapy against TAL1-driven T-cell acute lymphoblastic leukemia. *Genes Dev*. 2016;30:508–521.
21. Kim JH, Sharma A, Dhar SS, et al. UTX and MLL4 coordinately regulate transcriptional programs for cell proliferation and invasiveness in breast cancer cells. *Cancer Res*. 2014;74:1705–1717.
22. Paskeh MDA, Mehrabi A, Gholami MH, et al. EZH2 as a new therapeutic target in brain tumors: molecular landscape, therapeutic targeting and future prospects. *Biomed Pharmacother*. 2022;146:112532.
23. Song Y, Liu Y, Li ZM, et al. SHR2554, an EZH2 inhibitor, in relapsed or refractory mature lymphoid neoplasms: a first-in-human, dose-escalation, dose-expansion, and clini-

cal expansion phase 1 trial. *Lancet Haematol*. 2022;9:e493–e503.
24. Zauderer MG, Szlosarek PW, Le Moulec S, et al. EZH2 inhibitor tazemetostat in patients with relapsed or refractory, BAP1-inactivated malignant pleural mesothelioma: a multicentre, open-label, phase 2 study. *Lancet Oncol*. 2022;23:758–767.
25. Izutsu K, Ando K, Nishikori M, et al. Phase II study of tazemetostat for relapsed or refractory B-cell non-Hodgkin lymphoma with EZH2 mutation in Japan. *Cancer Sci*. 2021;112:3627–3635.
26. Sanchez A, Penault-Llorca F, Bignon YJ, Guy L, Bernard-Gallon D. Effects of GSK-J4 on JMJD3 histone demethylase in mouse prostate cancer xenografts. *Cancer Genomics Proteomics*. 2022;19:339–349.
27. D'Oto A, Fang J, Jin H, et al. KDM6B promotes activation of the oncogenic CDK4/6-pRB-E2F pathway by maintaining enhancer activity in MYCN-amplified neuroblastoma. *Nat Commun*. 2021;12:7204.
28. Kleszcz R, Skalski M, Krajka-Kuzniak V, Paluszczak J. The inhibitors of KDM4 and KDM6 histone lysine demethylases enhance the anti-growth effects of erlotinib and HS-173 in head and neck cancer cells. *Eur J Pharm Sci*. 2021;166:105961.
29. Zhang J, Ying Y, Li M, et al. Targeted inhibition of KDM6 histone demethylases eradicates tumor-initiating cells via enhancer reprogramming in colorectal cancer. *Theranostics*. 2020;10:10016–10030.
30. Li Y, Zhang M, Sheng M, et al. Therapeutic potential of GSK-J4, a histone demethylase KDM6B/JMJD3 inhibitor, for acute myeloid leukemia. *J Cancer Res Clin Oncol*. 2018;144:1065–1077.
31. Sui A, Xu Y, Li Y, et al. The pharmacological role of histone demethylase JMJD3 inhibitor GSK-J4 on glioma cells. *Oncotarget*. 2017;8:68591–68598.
32. Hsieh IY, He J, Wang L, et al. H3K27me3 loss plays a vital role in CEMIP mediated carcinogenesis and progression of breast cancer with poor prognosis. *Biomed Pharmacother*. 2020;123:109728.
33. Lin B, Lu B, Hsieh IY, et al. Synergy of GSK-J4 with doxorubicin in KRAS-mutant anaplastic thyroid cancer. *Front Pharmacol*. 2020;11:632.
34. Hong BJ, Park WY, Kim HR, et al. Oncogenic KRAS sensitizes lung adenocarcinoma to GSK-J4-induced metabolic and oxidative stress. *Cancer Res*. 2019;79:5849–5859.
35. Yildirim-Buharalioglu G. Lysine demethylase 6B regulates prostate cancer cell proliferation by controlling c-MYC expression. *Mol Pharmacol*. 2022;101:106–119.
36. Lochmann TL, Powell KM, Ham J, et al. Targeted inhibition of histone H3K27 demethylation is effective in high-risk neuroblastoma. *Sci Transl Med*. 2018;10:eaao4680.
37. Tschulakow AV, Schraermeyer U, Rodemann HP, Julien-Schraermeyer S. Establishment of a novel retinoblastoma (Rb) nude mouse model by intravitreal injection of human Rb Y79 cells - comparison of in vivo analysis versus histological follow up. *Biol Open*. 2016;5:1625–1630.
38. Mao Y, Sun Y, Wu Z, et al. Targeting of histone methyltransferase DOT1L plays a dual role in chemosensitization of retinoblastoma cells and enhances the efficacy of chemotherapy. *Cell Death Dis*. 2021;12:1141.
39. Kim JK, Kan G, Mao Y, et al. UHRF1 downmodulation enhances antitumor effects of histone deacetylase inhibitors in retinoblastoma by augmenting oxidative stress-mediated apoptosis. *Mol Oncol*. 2020;14:329–346.
40. Esteller M. Cancer epigenomics: DNA methylomes and histone-modification maps. *Nat Rev Genet*. 2007;8:286–298.
41. Kimura H. Histone modifications for human epigenome analysis. *J Hum Genet*. 2013;58:439–445.
42. Yin X, Yang S, Zhang M, Yue Y. The role and prospect of JMJD3 in stem cells and cancer. *Biomed Pharmacother*. 2019;118:109384.
43. Chu X, Zhong L, Yu L, et al. GSK-J4 induces cell cycle arrest and apoptosis via ER stress and the synergism between GSK-J4 and decitabine in acute myeloid leukemia KG-1a cells. *Cancer Cell Int*. 2020;20:209.
44. Lemaitre S, Poyer F, Marco S, et al. Looking for the most suitable orthotopic retinoblastoma mouse model in order to characterize the tumoral development. *Invest Ophthalmol Vis Sci*. 2017;58:3055–3064.
45. Antczak C, Kloepping C, Radu C, et al. Revisiting old drugs as novel agents for retinoblastoma: in vitro and in vivo antitumor activity of cardenolides. *Invest Ophthalmol Vis Sci*. 2009;50:3065–3073.
46. Dalpatraj N, Naik A, Thakur N. GSK-J4: an H3K27 histone demethylase inhibitor, as a potential anti-cancer agent. *Int J Cancer*. 2023;153:1130–1138.
47. Cao Z, Shi X, Tian F, et al. KDM6B is an androgen regulated gene and plays oncogenic roles by demethylating H3K27me3 at cyclin D1 promoter in prostate cancer. *Cell Death Dis*. 2021;12:2.
48. Gavet O, Pines J. Progressive activation of CyclinB1-Cdk1 coordinates entry to mitosis. *Dev Cell*. 2010;18:533–543.
49. Diao J, Wu C, Zhang J, et al. Loss of diacylglycerol kinase-zeta inhibits cell proliferation and survival in human gliomas. *Mol Neurobiol*. 2016;53:5425–5435.
50. Li Y, Luo X, Guo Q, et al. Discovery of N1-(4-((7-Cyclopentyl-6-(dimethylcarbamoyl)-7 H-pyrrolo[2,3- d]pyrimidin-2-yl)amino)phenyl)- N8-hydroxyoctanediamide as a novel inhibitor targeting cyclin-dependent kinase 4/9 (CDK4/9) and histone deacetlyase1 (HDAC1) against malignant cancer. *J Med Chem*. 2018;61:3166–3192.
51. Liu K, Xue B, Bai G, Zhang W. Downregulation of Diacylglycerol kinase zeta (DGKZ) suppresses tumorigenesis and progression of cervical cancer by facilitating cell apoptosis and cell cycle arrest. *Bioengineered*. 2021;12:1517–1529.
52. Twiddy D, Cain K. Caspase-9 cleavage, do you need it? *Biochem J*. 2007;405:e1–2.
53. Budihardjo I, Oliver H, Lutter M, Luo X, Wang X. Biochemical pathways of caspase activation during apoptosis. *Annu Rev Cell Dev Biol*. 1999;15:269–290.
54. Romani M, Daga A, Forlani A, Pistillo MP, Banelli B. Targeting of histone demethylases KDM5A and KDM6B inhibits the proliferation of temozolomide-resistant glioblastoma cells. *Cancers (Basel)*. 2019;11:878.
55. Lee SH, Kim O, Kim HJ, Hwangbo C, Lee JH. Epigenetic regulation of TGF-beta-induced EMT by JMJD3/KDM6B histone H3K27 demethylase. *Oncogenesis*. 2021;10:17.
56. Dolcet X, Llobet D, Pallares J, Matias-Guiu X. NF-kB in development and progression of human cancer. *Virchows Arch*. 2005;446:475–482.
57. Zhu Q, Enkhjargal B, Huang L, et al. Aggf1 attenuates neuroinflammation and BBB disruption via PI3K/Akt/NF-kappaB pathway after subarachnoid hemorrhage in rats. *J Neuroinflammation*. 2018;15:178.
58. Dalpatraj N, Naik A, Thakur N. Combination treatment of a phytochemical and a histone demethylase inhibitor-a novel approach towards targeting TGFbeta-induced EMT, invasion, and migration in prostate cancer. *Int J Mol Sci*. 2023;24:1860.

Investigative Ophthalmology & Visual Science